Measurements of rare Higgs decay couplings at the FCC-hh

Birgit Stapf[1*], Michele Selvaggi[1*] and Jan Eysermans[2*]

[1]CERN, Geneva, Switzerland.
[2]Massachusetts Institute of Technology, Cambridge, USA.

*Corresponding author(s). E-mail(s): birgit.stapf@cern.ch; michele.selvaggi@cern.ch; jan.eysermans@cern.ch;

1 Introduction

Measurements of the Higgs bosons properties, such as of its couplings with other Standard Model (SM) particles, at the Future Circular Collider(FCC) will allow to further understand its role in the SM and thereby in our universe. While the prospects for Higgs studies at the HL-LHC as well as the FCC-ee will already advance current levels of precision and insight significantly [1], [2], the hadron-hadron collider phase FCC-hh is crucial to complete the picture, by enabling high precision measurements of Higgs processes that remain out of reach for the nearer future. An example are the measurements of its couplings in rare decay modes, such as $H \to \mu\mu$, $H \to \gamma\gamma$ and $H \to Z\gamma$, which will be statistically limited at the FCC-ee. A previous study of these Higgs decay modes was performed as part of the Conceptual Design Report (CDR) [3, 4] of the FCC-hh and detailed in Ref. [5], assuming the CDR baseline operation at $\sqrt{s}=$ 100 TeV and an integrated luminosity of 30 ab^{-1}. This study focused on analyzing Higgs production at large transverse momenta, p_{T}^{H} , exploiting the fact that with the expected FCC-hh dataset even this region of phase space will be abundantly populated, and that experimental uncertainties in this region are typically smaller than at lower p_{T}^{H} , where reconstruction of physics objects is more difficult due to e.g. trigger thresholds or the impact of pile-up. In order to keep the projections robust and largely independent of assumptions on the levels of theoretical (and to some extent experimental) uncertainties in the future, measurements of Higgs decay channels within similar fiducial regions were combined into a measurement of the production ratio. Common theoretical uncertainties regarding the production cross-section, as well as experimental uncertainties deriving from the luminosity measurement, vanish in such a ratio.

In this way, the sub-percent level precision on the Higgs couplings in the $H \to \mu\mu$, $H \to \gamma\gamma$ and $H \to Z\gamma$ with CDR baseline FCC-hh scenario are achieved.

This note presents on update to these Higgs boson studies in rare decay modes at the FCC-hh. As a first case study, the measurement of the Higgs to muon coupling exploiting the ratio of $H \to \mu\mu$ over $H \to ZZ* \to 4\mu$ production is revisited for the updated FCC-hh baseline scenario, which assumes an integrated luminosity of 30 ab^{-1} at a center-of-mass energy of $\sqrt{s} = 84$ TeV. While the previous results were obtained from a simple counting experiment, the new strategy exploits the different shapes of the $m_{\mu\mu}$ invariant mass and $p_{T,\mu\mu}$ distributions between signal and background in a 2D template fit. Moreover the estimation of the experimental systematic uncertainties was further refined, using p_T-dependent scale factors capturing the reconstruction efficiency uncertainties of each muon, and measuring the non-resonant background in a data-driven way from the large statistics in the sidebands. Completion of this update by expanding the newly defined, more sensitive analysis strategy also to the $H \to \gamma\gamma$ and $H \to Z\gamma$ channels as well as studying the complete set of alternative FCC-hh running scenarios detailed in Ref. [6] is expected within the coming months.

2 Event generation

The analysis relies on Monte Carlo generated events for both the signal and the background processes considered. In general, all samples are generated at leading-order (LO) precision using `MadGraph5_aMC@NLO` [7] with `NNPDF3.0NLO` [8]. `Pythia8` [9] is used for the Higgs boson decay into two photons, parton showering, and hadronization effects. Since the analysis aims to exploit the large statistics of events with large transverse momentum of the Higgs to di-photon candidate, the generation of signal and dominant background processes accounts for additional jets in the matrix element, as specified in the following. The matching between matrix element and parton shower jets employed follows the MLM-scheme described in [10].

For the Higgs boson signal, its leading production modes of gluon-gluon fusion (ggH), vectorboson fusion (VBF H), top-quark pair associated production ($t\bar{t}H$) and the production in association with a vector boson (VH), are considered. The event generation of ggH and VH events includes contributions up-to and including two additional jets in the matrix element, while that of VBF H and $t\bar{t}H$ events considers only up to one additional jet. For each production mode the respective LO cross-section is corrected to higher orders using k-factors derived from the most accurate predictions in [11] for the studies at 100 TeV. These k-factors are thus assumed to be independent of the center of mass energy.

In terms of background, only the dominant continuum backgrounds processes are considered: that is the $\mu\mu$ continuum in the $H \to \mu\mu$ analysis, and the 4ℓ continuum in the $H \to ZZ* \to 4\mu$ analysis. The generation of the former includes up to two additional MLM-matched jets in the matrix element, while the latter stops at one additional MLM-matched jet. In both cases, an invariant mass of the Higgs boson decay products in the range of $50 < m^{\mathrm{gen}}_{\mu\mu\,\mathrm{or}\,4\mu} < 200$ GeV at generator level, in order to increase MC statistics in the phase space region of interest for the analysis. The LO $\mu\mu$ continuum cross-section is corrected with a k-factor of 1.2 following Ref. [5] and that of the 4ℓ continuum with a k-factor of 1.6 extracted from the predictions in Ref. [12]. Again, these k-factors were evaluated using the 100 TeV cross-sections. Background contributions from mis-identified objects (fakes) were not considered in the analysis.

Table 1 summarizes the respective cross-sections of each signal and background process considered, for the various center of mass energies studied, including all correction-factors as discussed above.

	Cross-section in pb, for $\sqrt{s}$ =			
Process	72 TeV	84 TeV	100 TeV	120 TeV
Signals				
ggH	543	657	802	999
VBF H	45	54	69	86
$t\bar{t}H$	19	25	33	45
VH	19	22	27	32
Backgrounds				
$\mu\mu$ continuum	257	288	339	385
4ℓ continuum	0.050	0.056	0.064	0.073

Table 1: Overview of total signal and background cross-sections at different center of mass energies. The background cross-section refer to the fiducial region, with $50 < m^{\text{gen}}_{\mu\mu\,\text{or}\,4\mu} < 200$ GeV.

3 Event Reconstruction and Selection

A reference detector for the FCC-hh has been designed and described in the CDR. All samples considered in this analysis rely on a fast simulation of this detector design with the DELPHES tool [13], which describes the response of the detector components using parameterizations of the resolution and efficiency functions. Details on the specific assumptions and parameterizations for the FCC-hh reference detector scenario can be found in Ref. [14], while Ref. [13] describes the generalities of object reconstruction in DELPHES. The muons as used in this analysis, are reconstructed with a relative momentum resolution of the percent-level, and an efficiency ranging from 90-97%. Although no direct pile-up overlay is considered in the fast simulations performed here, the impact of pile-up at LHC levels is implicitly considered through the DELPHES parameterizations.

For the technical implementation of the event generation and simulation, the common software stack for future facilities provided by the KEY4HEP framework [15, 16] is employed. In particular, the samples used here are in EDM4HEP format [17]. The complete list of generated samples can be found in Ref. [18]. The samples are further processed with the FCCANALYSES framework [19], implementing the selection of final state objects and events based on the criteria outlined in Table 2.

	$H \to \mu\mu$	$H \to ZZ* \to 4\mu$
Muon transverse momenta	$p_{\mathrm{T}}(\mu_1) > 20$ GeV $p_{\mathrm{T}}(\mu_2) > 20$ GeV	$p_{\mathrm{T}}(\mu_1) > 20$ GeV $p_{\mathrm{T}}(\mu_2) > 10$ GeV $p_{\mathrm{T}}(\mu_3) > 7$ GeV $p_{\mathrm{T}}(\mu_3) > 5$ GeV
Muon pseudorapidity	$\|\eta(\mu) < 4$	$\|\eta(\mu) < 4$
Muon isolation	rel. Iso. $(\mu) < 0.2$	rel. Iso. $(\mu) < 0.2$
Z decay candidates	-	$40 < m_{\mu\mu}$ (leading pair) < 120 GeV $12 < m_{\mu\mu}$ (subleading pair) < 120 GeV

Table 2: Summary of object and event selection criteria per analysis.

4 Analysis strategy and systematic uncertainties

The selected events are further split into different bins of the transverse momentum of the Higgs candidate, $p_T^{\mu\mu}$ and $p_T^{4\mu}$ for the $H \to \mu\mu$ and $H \to ZZ* \to 4\mu$ analysis respectively.

Figure 1 shows the resulting distributions for the $H \to \mu\mu$ analysis, and Figure 2 those of the $H \to ZZ* \to 4\mu$ analysis.

In each bin, a systematic uncertainty to account for the muon reconstruction efficiencies is determined from the parametrization first introduced in Ref. [5] and applied to the signals. The corresponding relative uncertainty value per muon is taken from this parametrization depending on its transverse momentum, and an overall scalefactor for the event is defined as the multiplication of the individual muon uncertainties. A normalisation uncertainty, averaging across all events in the bin, is then determined from reweighting the invariant mass distributions in each bin with scalefactor and comparing to the nominal case. Figure **??** shows the value of this muon reconstruction efficiency systematic per bin for each analysis. In the template fit, this uncertainty is described by a single nuisance parameter, therefore correlating the measurements across the p_{T} bins as well as between the $H \to \mu\mu$ and $H \to ZZ* \to 4\mu$ analysis. Additionally, a flat uncertainty of 1% on the luminosity measurement is assumed in the standalone $H \to \mu\mu$ and $H \to ZZ* \to 4\mu$ results, is applied on the signals. In the ratio of $H \to \mu\mu$ over $H \to ZZ* \to 4\mu$ this uncertainty fully cancels.

As the background normalisation can be determined from the data sidebands with high precision, no further uncertainties on the background processes are assumed. Instead, a free floating normalisation factor for each background is used in the fit.

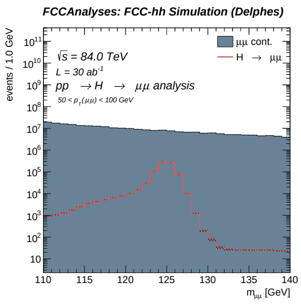

(a) $50 \leq p_T^{\mu\mu} < 100$ GeV

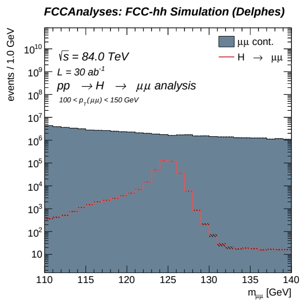

(b) $100 \leq p_T^{\mu\mu} < 150$ GeV

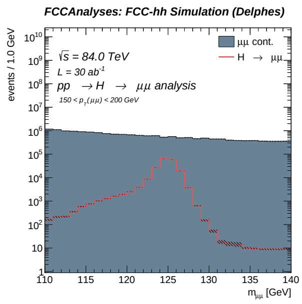

(c) $150 \leq p_T^{\mu\mu} < 200$ GeV

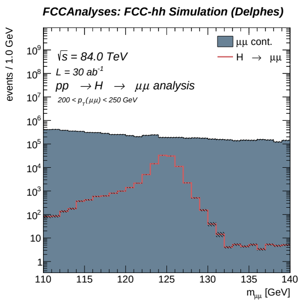

(d) $200 \leq p_T^{\mu\mu} < 250$ GeV

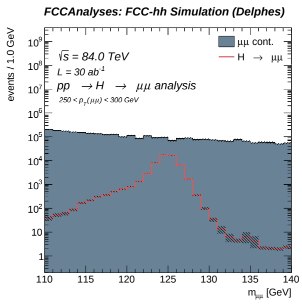

(e) $250 \leq p_T^{\mu\mu} < 300$ GeV

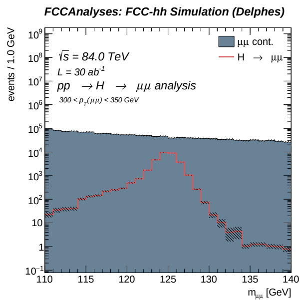

(f) $300 \leq p_T^{\mu\mu} < 350$ GeV

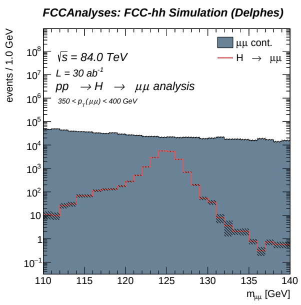

(g) $350 \leq p_T^{\mu\mu} < 400$ GeV

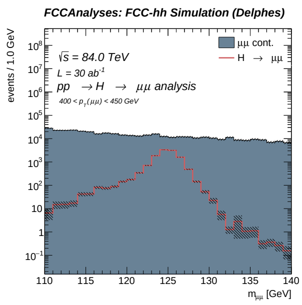

(h) $400 \leq p_T^{\mu\mu} < 450$ GeV

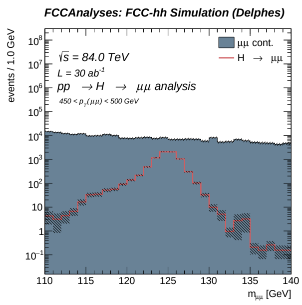

(i) $450 \leq p_T^{\mu\mu} < 500$ GeV

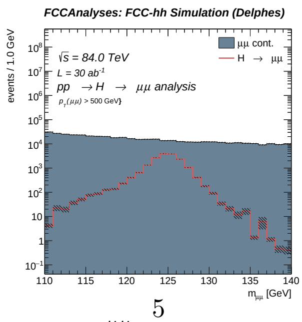

(j) $p_T^{\mu\mu} > 500$ GeV

Fig. 1: $H \to \mu\mu$ analysis: Distributions of $m_{\mu\mu}$ for the Higgs signals (red) and the $\mu\mu$ continuum background (blue), in the different bins of $p_T^{\mu\mu}$.

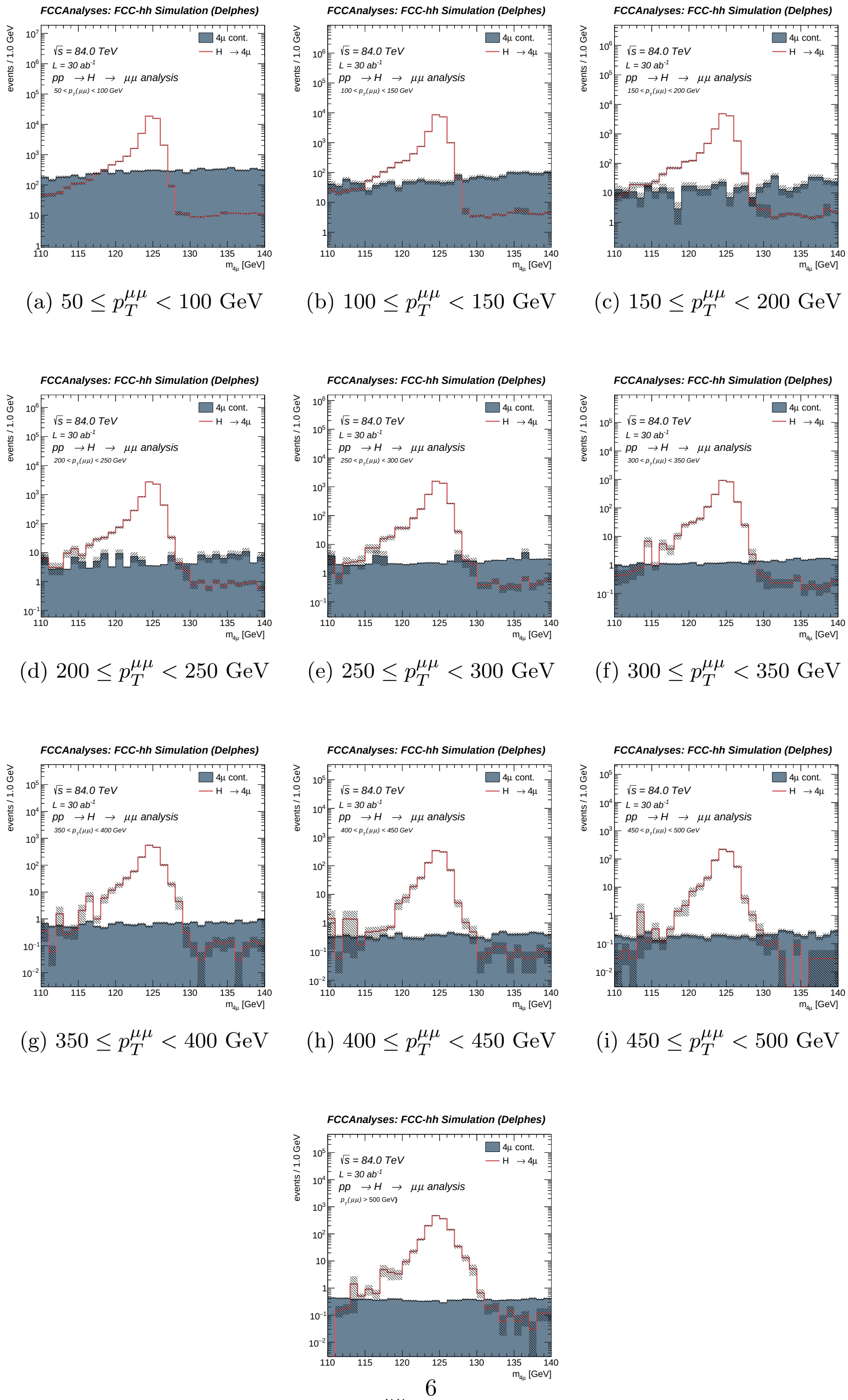

(a) $50 \leq p_T^{\mu\mu} < 100$ GeV (b) $100 \leq p_T^{\mu\mu} < 150$ GeV (c) $150 \leq p_T^{\mu\mu} < 200$ GeV

(d) $200 \leq p_T^{\mu\mu} < 250$ GeV (e) $250 \leq p_T^{\mu\mu} < 300$ GeV (f) $300 \leq p_T^{\mu\mu} < 350$ GeV

(g) $350 \leq p_T^{\mu\mu} < 400$ GeV (h) $400 \leq p_T^{\mu\mu} < 450$ GeV (i) $450 \leq p_T^{\mu\mu} < 500$ GeV

(j) $p_T^{\mu\mu} > 500$ GeV

Fig. 2: $H \rightarrow ZZ* \rightarrow 4\mu$ analysis: Distributions of $m_{4\mu}$ for the Higgs signals (red) and the 4ℓ continuum background (blue), in the different bins of $p_T^{4\mu}$.

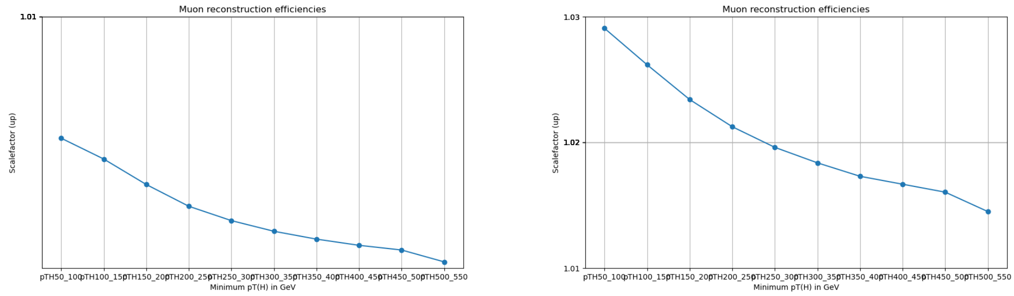

(a) $H \to \mu\mu$ analysis (b) $H \to ZZ* \to 4\mu$ analysis

Fig. 3: Evolution of the p_{T}-dependent muon reconstruction uncertainty in the bins on the Higgs candidate transverse momentum. Only the "up" variation is shown, the uncertainty is assumed to be symmetric.

5 Results

Figure 4 shows the differential measurements of the ratio $\mathcal{B}(\mathrm{H} \to \mu\mu)/\mathcal{B}(\mathrm{H} \to \mu\mu\mu\mu)$ for different values of $\mathrm{p_T(H)}$ for the new baseline scenario of 84 TeV, and the CDR baseline scenario of 100 TeV. Since the analysis is systematically dominated, the loss of precision from the simultaneous fit across all bins at the lower center of mass energy is insignificant.

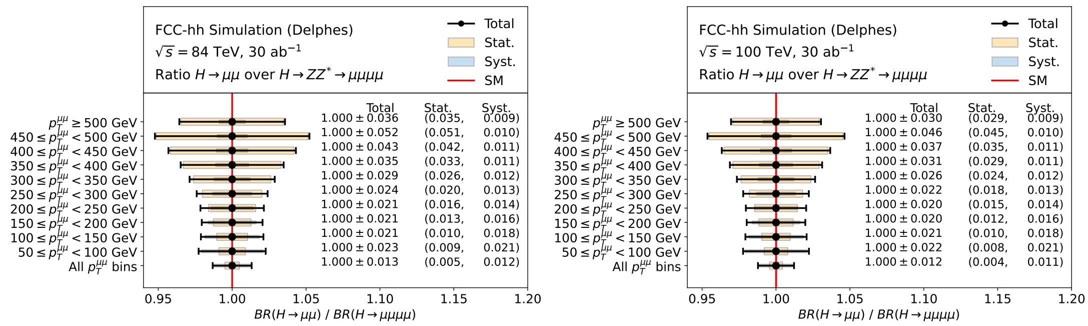

(a) FSR baseline of 84 TeV (b) CDR baseline of 100 TeV

Fig. 4: Differential measurements of the ratio $\mathcal{B}(\mathrm{H} \to \mu\mu)/\mathcal{B}(\mathrm{H} \to \mu\mu\mu\mu)$ for different values of $\mathrm{p_T(H)}$ and the different operating scenarios.

6 Conclusion

Acknowledgements

This work has been partly supported by the Future Circular Collider Innovation Study (FCCIS) project, that has received funding from the European Union's Horizon 2020 research and innovation programme under grant No 951754.

References

[1] M. Selvaggi, A. Blondel, J. Eysermans. Prospects in Electroweak, Higgs and Top physics at FCC (2025). https://doi.org/10.17181/n78xk-qcv56

[2] G. Wilkinson, A. Blondel, P. Janot, C. Grojean, S. Rajagopalan. The FCC integrated programme: a physics manifesto (2025). https://doi.org/10.17181/3kaxg-ejn91

[3] A. Abada, et al., FCC Physics Opportunities: Future Circular Collider Conceptual Design Report Volume 1. Eur. Phys. J. C **79**, 474 (2019). https://doi.org/10.1140/epjc/s10052-019-6904-3

[4] A. Abada, et al., FCC-hh: The Hadron Collider: Future Circular Collider Conceptual Design Report Volume 3. Eur. Phys. J. ST **228**, 755 (2019). https://doi.org/10.1140/epjst/e2019-900087-0

[5] B.D.M.E.F.P.H.C.H.D.J.M.M.G.O.M.S.A.S.M.T.M.V. L. Borgonovi, S. Braibant, Higgs measurements at FCC-hh. Tech. rep., CERN, Geneva (2018). URL https://cds.cern.ch/record/2642471

[6] F. Zimmermann. Scenarios for the FCC-hh (2025). https://doi.org/10.5281/zenodo.14934133

[7] J. Alwall, R. Frederix, S. Frixione, V. Hirschi, F. Maltoni, O. Mattelaer, H.S. Shao, T. Stelzer, P. Torrielli, M. Zaro, The automated computation of tree-level and next-to-leading order differential cross sections, and their matching to parton shower simulations. JHEP **07**, 079 (2014). https://doi.org/10.1007/JHEP07(2014)079. arXiv:1405.0301 [hep-ph]

[8] R.D. Ball, et al., Parton distributions for the LHC Run II. JHEP **04**, 040 (2015). https://doi.org/10.1007/JHEP04(2015)040. arXiv:1410.8849 [hep-ph]

[9] C. Bierlich, et al., A comprehensive guide to the physics and usage of PYTHIA 8.3. SciPost Phys. Codeb. **2022**, 8 (2022). https://doi.org/10.21468/SciPostPhysCodeb.8. arXiv:2203.11601 [hep-ph]

[10] M.L. Mangano, M. Moretti, F. Piccinini, M. Treccani, Matching matrix elements and shower evolution for top-pair production in hadronic collisions. JHEP

2007(01), 013–013 (2007). https://doi.org/10.1088/1126-6708/2007/01/013. URL http://dx.doi.org/10.1088/1126-6708/2007/01/013

[11] R. Contino, D. Curtin, A. Katz, M.L. Mangano, G. Panico, M.J. Ramsey-Musolf, G. Zanderighi, C. Anastasiou, W. Astill, G. Bambhaniya, J.K. Behr, W. Bizon, P.S.B. Dev, D. Bortoletto, D. Buttazzo, Q.H. Cao, F. Caola, J. Chakrabortty, C.Y. Chen, S.L. Chen, D. de Florian, F. Dulat, C. Englert, J.A. Frost, B. Fuks, T. Gherghetta, G. Giudice, J. Gluza, N. Greiner, H. Gray, N.P. Hartland, C. Issever, T. Jelinski, A. Karlberg, J.H. Kim, F. Kling, A. Lazopoulos, S.J. Lee, Y. Liu, G. Luisoni, J. Mazzitelli, B. Mistlberger, P. Monni, K. Nikolopoulos, R.N. Mohapatra, A. Papaefstathiou, M. Perelstein, F. Petriello, T. Plehn, P. Reimitz, J. Ren, J. Rojo, K. Sakurai, T. Schell, F. Sala, M. Selvaggi, H.S. Shao, M. Son, M. Spannowsky, T. Srivastava, S.F. Su, R. Szafron, T. Tait, A. Tesi, A. Thamm, P. Torrielli, F. Tramontano, J. Winter, A. Wulzer, Q.S. Yan, W.M. Yao, Y.C. Zhang, X. Zhao, Z. Zhao, Y.M. Zhong, Physics at a 100 tev pp collider: Higgs and ew symmetry breaking studies (2016). arXiv:1606.09408 [hep-ph]

[12] M. Mangano, M. Mangano, *Physics at the FCC-hh, a 100 TeV pp collider*. CERN Yellow Reports: Monographs (CERN, Geneva, 2017). https://doi.org/10.23731/CYRM-2017-003. URL https://cds.cern.ch/record/2270978

[13] de Favereau, J. and Delaere, C. and Demin, P. and Giammanco, A. and Lemaître, V. and Mertens, A. and Selvaggi, M., DELPHES 3, A modular framework for fast simulation of a generic collider experiment. JHEP **02**, 057 (2014). https://doi.org/10.1007/JHEP02(2014)057. arXiv:1307.6346 [hep-ex]

[14] M. Selvaggi, B. Stapf. A Delphes parameterisation of the FCC-hh detector (2025). https://doi.org/10.17181/71pv5-tvf87

[15] P. Fernandez Declara, et al., The Key4hep turnkey software stack for future colliders. PoS **EPS-HEP2021**, 844 (2022). https://doi.org/10.22323/1.398.0844

[16] B. Francois, G. Ganis, *The FCC software for PED studies* (2024). https://doi.org/10.17181/8k0c4-nkr70

[17] *EDM4hep data model*. https://edm4hep.web.cern.ch/

[18] B. Stapf, J. Smiesko. List of fcc_v07 official FCC-hh production samples (2025). https://fcc-physics-events.web.cern.ch/fcc-hh/delphes/fcc-v07/ii or https://fcc-physics-events.web.cern.ch/fcc-hh/Delphesevents_fcc_v07/II.php

[19] C. Helsens, E. Perez, M. Selvaggi, V. Volkl, L. Forthomme, J. Munch Torndal. Hep-fcc/fccanalyses: v0.10.0 (2024). https://doi.org/10.5281/zenodo.13871482. URL https://doi.org/10.5281/zenodo.13871482